

# UC Berkeley

## UC Berkeley Previously Published Works

### Title

Platinum nanoparticle induced nanoionic effects on electrical conduction in strontium cerate and zirconate

### Permalink

<https://escholarship.org/uc/item/7v416180>

### Journal

Journal of Solid State Electrochemistry, 23(3)

### ISSN

1432-8488

### Authors

Takamura, Yasuhiro  
Leonard, Kwati  
Luo, Aileen  
[et al.](#)

### Publication Date


2019-03-01

### DOI

10.1007/s10008-018-04188-z

Peer reviewed

# Platinum nanoparticle induced nanoionic effects on electrical conduction in strontium cerate and zirconate

Yasuhiro Takamura<sup>1,2</sup>  Kwati Leonard<sup>2</sup> · Aileen Luo<sup>3</sup> · Lane W. Martin<sup>3,4</sup> · Hiroshige Matsumoto<sup>2</sup>

## Abstract

Heterointerfaces introduce unique localized defects into ionic conductors. This study explores the nanoionic characteristics exhibited by the proton-conducting oxides  $\text{SrZr}_{0.9}\text{Y}_{0.1}\text{O}_{3-\delta}$  and  $\text{SrCe}_{0.95}\text{Yb}_{0.05}\text{O}_{3-\delta}$  including finely dispersed precipitated platinum nanoparticles. The electrical conductivity of both the platinum-doped oxides revealed reversible nanoionic phenomena caused by the exsolution of the platinum in the form of platinum nanoparticles, at 0.5 vol% relative to the metal oxides, and dissolution in response to a change in gas atmosphere. In comparison with the original conductivity of  $\text{SrZr}_{0.9}\text{Y}_{0.1}\text{O}_{3-\delta}$  and  $\text{SrCe}_{0.95}\text{Yb}_{0.05}\text{O}_{3-\delta}$ , the conductivity of platinum-doped  $\text{SrZr}_{0.9}\text{Y}_{0.1}\text{O}_{3-\delta}$  decreased significantly in a wet hydrogen atmosphere, whereas platinum-doped  $\text{SrCe}_{0.95}\text{Yb}_{0.05}\text{O}_{3-\delta}$  showed almost no decrease in conductivity in the same atmosphere. The different responses of the two materials to the change in gas atmosphere are discussed in relation to the precipitation of platinum nanoparticles.

## Introduction

Solid oxide ionic conductors are major components in electrochemical devices, such as fuel cells and steam electrolyzers [1–4]. The ionic conductivity of these solid oxides is proportional to the product of the concentration and mobility of their ionic charge carriers. The design of

such materials should therefore focus on increasing one or both of these properties. Point defects are chemical species that work as ionic charge carriers [5], and chemical compositions are chosen to increase their concentration. Mobility is related to crystal symmetry and lattice constants [6], and thus, the crystal structure is an important factor in mobility.

A reported approach to increase ionic conductivity is the use of heterointerfaces [7–10]. At the interface of two materials with different work functions, a space-charge layer forms that alters the defect equilibria and changes the charge-carrier concentration. Another possibility is the generation of strain at the interface, which changes the mobility and defect concentration of ionic charge carriers. These effects can be used to enhance the ionic conductivity in this class of materials. This study investigated changes in the electrical properties of proton-conducting oxides upon homogeneously dispersing platinum nanoparticles. The change is compared between two different proton conductors:  $\text{SrZr}_{0.9}\text{Y}_{0.1}\text{O}_{3-\delta}$  (SZY) and  $\text{SrCe}_{0.95}\text{Yb}_{0.05}\text{O}_{3-\delta}$  (SCYb); the reason for the choice of these is mentioned at the end of this section.

Proton conductivity in SZY (SCYb) originates from the trivalent cation  $\text{Y}^{3+}$  ( $\text{Yb}^{3+}$ ) being substituted for  $\text{Zr}^{4+}$

(Ce<sup>4+</sup>) at the *B* site of the  $A^{2+}B^{4+}O_3$  perovskite structure to generate oxygen vacancies, where the following defect equilibria hold:



Here,  $V_{\text{O}}^{\cdot\cdot}$ ,  $\text{O}_{\text{O}}^{\times}$ ,  $h^{\cdot}$ , and  $\text{H}_i^{\cdot}$  are described using Kröger-Vink notation, denoting oxygen vacancies, lattice oxygen, electron holes, and protons, respectively.  $\text{H}_i^{\cdot}$  is covalently bonded to one lattice oxygen while interacting with other neighboring oxygen atoms via hydrogen bonds, and can move by changing the covalent/hydrogen bonding oxygen [11]. The sum of the two equilibrium equations yields the following:



Thus, the formation of a protonic charge carrier is, overall, the result of hydration of an oxide-ion vacancy. By applying the following equilibrium for water formation in Eqs. (2) to (4), we can obtain Eq. (5).



These defect equilibria indicate that several conduction species can serve as charge carriers, depending on the gas atmosphere and temperature. As shown in Eq. (3), the concentration of protons is a function of the partial pressure of water vapor and is approximately independent of the partial pressure of oxygen [12–14]. An exception is the increase in the proton concentration in strontium cerate upon the decrease in the partial pressure of oxygen [15, 16] and is discussed in later section. The equilibrium in Eq. (3) will shift to the left as temperature increases and is accompanied by the appearance of an oxide ion contribution as the charge carrier. In this report, all measurements are carried out under conditions where the proton is assumed to be the major charge carrier. To ensure that this criterion is satisfied, the transport numbers of proton and oxide ions in SZY and SCYb were experimentally determined by hydrogen and steam concentration cell measurements, and are consistent with results reported previously [17–19].

We have reported that a solid solution of platinum in SZY can be prepared by adding a platinum complex to an aqueous precursor during wet chemical synthesis of the material [20, 21]. The obtained material reversibly exsolved metallic platinum as nanoparticles from the crystal lattice upon exposure to a reducing atmosphere, and

dissolved them back into the crystal lattice under an oxidizing atmosphere. Generation of platinum nanoparticles at 0.5 vol% platinum in SZY upon exposure to a reducing atmosphere leads to a significant reduction in electrical conductivity compared with the original conductivity of undoped SZY. The reduction in conductivity can be explained by the formation of a space-charge layer formed at the interface of the SZY phase with the platinum nanoparticles, as schematically shown (Fig. 1 (a) and (a')). If the Fermi level of SZY is originally lower than that of platinum, SZY will be negatively charged at the interface with platinum to match the Fermi level. The hole concentration in SZY then decreases, and the proton concentration also decreases to maintain the equilibrium shown in Eq. (5) [20, 21]. It is reasonable to assume the equilibrium of ionic defects, i.e., the electrochemical potentials of the ionic species should be equalized between the Pt and oxide phases. Since the ionic species such as protons cannot exist in platinum apparently, the equilibrium will be achieved virtually with only a small concentration change to reach their equilibriums between the two phases. Hence, formation of space charge associated with their movement can be ignored in effect, and thus, we can consider that the space charge is presumably derived from the equilibrium of the Fermi level.

Depletion of the protonic charge carriers may affect both the conductivity and the electrocatalytic activity of the platinum electrodes used in proton-conducting materials. It has been reported that platinum electrodes perform inadequately when used in combination with SZY [22]. This could possibly be attributed to the depletion of protonic charge carriers at the interface with the platinum electrode where the electrode reaction occurs. The electrode activity of platinum is not always poor for proton conductors. In fact, platinum electrodes work well with SCYb [17, 18, 22]. This observation suggests that a platinum interface may work differently with strontium cerate. In this study, the materials used were selected based on the reported platinum electrode overvoltage for SZY and SCYb [22]. We investigated the abovementioned nanoionic phenomena on SCYb to understand these effects in comparison with the SZY results.

## Experimental

### Sample preparation

$\text{SrZr}_{0.9}\text{Y}_{0.1}\text{O}_{3-\delta}$  and  $\text{SrCe}_{0.95}\text{Yb}_{0.05}\text{O}_{3-\delta}$  and version including platinum nanoparticles (Pt-SZY, Pt-SCYb) were prepared by a combustion synthesis method. The amount of platinum is equivalent to 0.5 vol% in the form of exsolved metal relative to the proton-conducting metal oxide phase. Stoichiometric amounts of the following

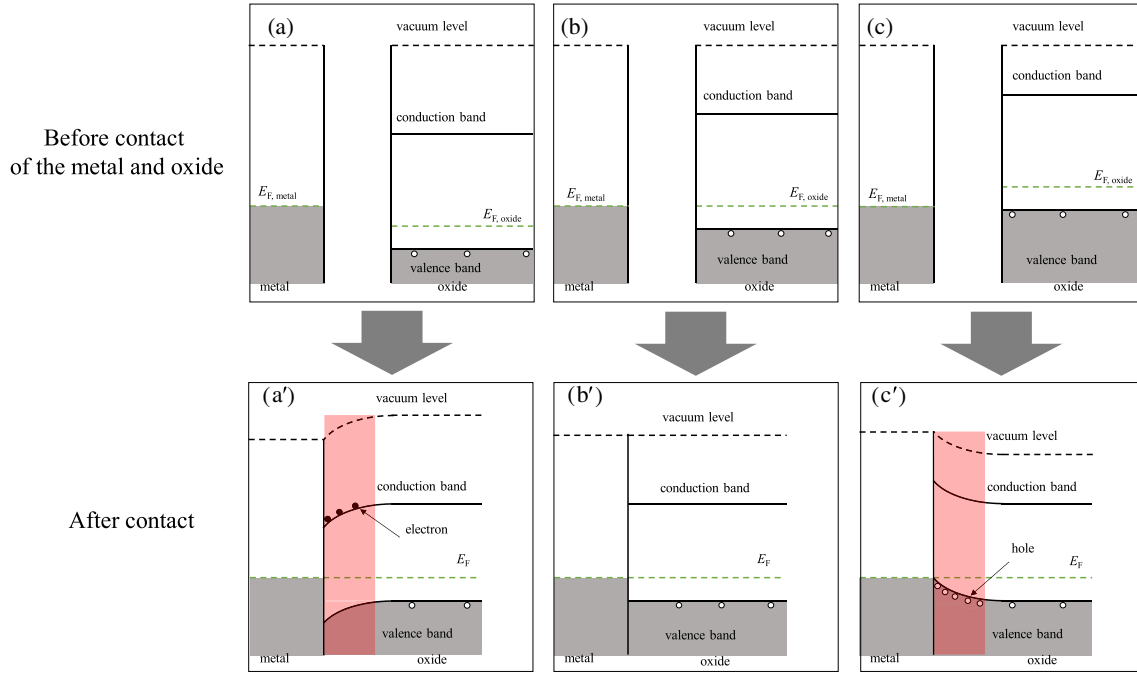


**Fig. 1** Schematic diagram of band bending models. (a) Before contact,  $E_{F,metal}$  is larger than  $E_{F,oxide}$ , and (a') after contact, the hole concentration of oxide decreases in the vicinity of the heterointerface. (b) Before contact,  $E_{F,metal}$  is the same as  $E_{F,oxide}$ , and (b') after contact, the hole

concentration of oxide is maintained in the vicinity of the heterointerface. (c) Before contact,  $E_{F,metal}$  is smaller than  $E_{F,oxide}$ , and (c') after contact, the hole concentration of the oxide increases in the vicinity of the heterointerface

materials with an excess of *B* site by added platinum were dissolved in water and mixed homogeneously:  $\text{Sr}(\text{NO}_3)_2$  (Soekawa Chem. Co., Ltd., 99.9%),  $\text{ZrO}(\text{NO}_3)_2 \cdot 2\text{H}_2\text{O}$  (Kishida Chem. Co., Ltd., 99.0%),  $\text{Y}(\text{NO}_3)_3 \cdot 6\text{H}_2\text{O}$  (Sigma-Aldrich, 99.8%),  $\text{Ce}(\text{NO}_3)_3 \cdot 6\text{H}_2\text{O}$  (Kanto Chem. Co., Inc., 99.99%),  $\text{Yb}(\text{NO}_3)_3 \cdot 6\text{H}_2\text{O}$  (Mitsuiwa Chem. Co., Ltd., 99.9%), and  $\text{Pt}(\text{NH}_3)_4(\text{NO}_3)_2$  (Sigma-Aldrich, 99.95%). EDTA (Wako Pure Chem. Industries Ltd., 99.0%), citric acid (Wako Pure Chem. Industries Ltd., 99.5%), aqueous ammonia solution (Kishida Chem. Co., Ltd., 28.0%  $\text{NH}_3$  in  $\text{H}_2\text{O}$ ), and ammonium nitrate (Kishida Chem. Co., Ltd., 99.0%) were also added to promote polymerization and combustion. The solution was heated under constant stirring until ignition occurred. The obtained powder was calcined in air for 10 h at 1100 °C and then subjected to planetary ball milling in ethanol for 1 h. The dried and sieved powder was molded into disks or rectangular bars, isostatically pressed at 250 MPa, and then sintered in air for 10 h. The disk-shaped SZY and SCYb samples, which were used to investigate transport numbers, were sintered at 1600 °C. For the platinum-containing specimens, platinum was expected to dissolve into a solid solution during sintering in air. To find the appropriate sintering temperature, Pt-SCYb was sintered at different temperatures and the presence or absence of platinum precipitation was examined using X-ray diffraction (XRD Ultima IV, using Cu-K $\alpha$  radiation X-ray source). SZY and Pt-SZY were sintered at 1350 °C,

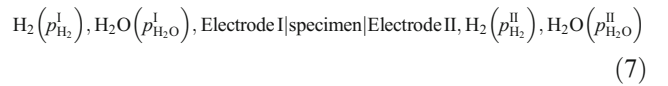
as previously reported [21], whereas SCYb and Pt-SCYb were sintered at 1150 °C, as determined in this work. Transmission electron microscopy (TEM JEM-3200FSK) was used at 300 kV to observe the precipitated platinum in Pt-doped SCYb after exposure to wet 1%  $\text{H}_2$ .

## Determination of transport numbers

The transport number for a conducting species, *i*, is defined

$$t_i = \sigma_i / \sigma_T \quad (6)$$

where  $t_i$  and  $\sigma_i$  are, respectively, the transport number and partial conductivity of species *i* and  $\sigma_T$  is the total conductivity. The following electrochemical cell consisting of metal electrodes and a dense specimen was used in determining the ionic and electronic transport numbers:



where  $p_{\text{H}_2\text{O}}^{\text{I or II}}$  indicates the partial pressure of water vapor or hydrogen introduced in the electrode compartment I or II. A disk-shaped electrolyte (diameter approx. 13 mm; thickness approx. 0.5 mm) with porous platinum electrodes was placed between the ceramic tubes with glass gaskets (Corning Pyrex 7740) to construct the test cell. In order to melt the glass, the components were heated at 950 °C.

The EMF of the cell is expressed by the following equation [23]:

$$E = t_{\text{O}^{2-}} \frac{RT}{2F} \ln \frac{p_{\text{H}_2\text{O}}^{\text{II}}}{p_{\text{H}_2\text{O}}^{\text{I}}} - (t_{\text{O}^{2-}} + t_{\text{H}^+}) \frac{RT}{2F} \ln \frac{p_{\text{H}_2}^{\text{II}}}{p_{\text{H}_2}^{\text{I}}} \quad (8)$$

where  $R$ ,  $T$ , and  $F$  are the gas constant, temperature, and Faraday constant, respectively.

(i) Hydrogen-concentration cell

When  $p_{\text{H}_2\text{O}}^{\text{I}} = p_{\text{H}_2\text{O}}^{\text{II}}$ , the first term in Eq. (7) is zero, and so, the EMF refers to the total ionic transport number, that is,  $t_{\text{O}^{2-}} + t_{\text{H}^+}$ . Experimentally, the hydrogen partial pressure was controlled by dilution with argon, to yield  $p_{\text{H}_2}^{\text{I}} = 1\text{--}98$  kPa,  $p_{\text{H}_2}^{\text{II}} = 1$  kPa,  $p_{\text{H}_2\text{O}}^{\text{I}} = p_{\text{H}_2\text{O}}^{\text{II}} = 1.9$  kPa.

(ii) Steam-concentration cell

When  $p_{\text{H}_2}^{\text{I}} = p_{\text{H}_2}^{\text{II}}$ , the second term in Eq. (7) is zero, and so, the EMF responds to the oxide-ion transport number, that is,  $t_{\text{O}^{2-}}$ . Experimentally,  $p_{\text{H}_2}^{\text{I}} = p_{\text{H}_2}^{\text{II}} = 1$  kPa,  $p_{\text{H}_2\text{O}}^{\text{I}} = 1.9$  kPa,  $p_{\text{H}_2\text{O}}^{\text{II}} = 0.65\text{--}1.9$  kPa.

### Electrical conductivity measurement

The electrical conductivity was measured by an AC four-probe method on a rectangular bar specimen (12 mm × 3 mm × 1 mm) in the temperature range of 400–800 °C. Porous platinum electrodes were prepared by applying platinum paste which was subsequently annealed in air at 950 °C and attached to a platinum lead wire. Gas streams of 21% O<sub>2</sub>-Ar, Ar, and 1% H<sub>2</sub>-Ar were applied sequentially for the conductivity measurement. All gases were humidified with water vapor at a pressure of 1.9 kPa (1.9% of the inflow gases). Electrochemical impedance spectroscopy (EIS) measurements were carried out on all samples, beginning with a wet argon atmosphere. Samples were heated at a ramp rate of 5 °C/min to 400 °C, and the temperature was held until the resistance value stabilized. Then, the impedance measurement was conducted as the gases were changed in the order air → Ar → 1% H<sub>2</sub> → Ar → air while maintaining the water vapor pressure at 1.9 kPa. This was repeated from 800 °C down to 400 °C at intervals of 100 °C. All conductivity measurements were carried out with a VersaStat 4 (Princeton Applied Research) in a frequency range of 1 × 10<sup>6</sup> to 1 Hz.

### Photoelectron spectroscopy

UPS measurements were performed to evaluate the work functions of SZY and SCYb using a PHI 5000 VersaProve II (ULVAC-PHI, inc). The UPS spectra were collected using a He I source ( $h\nu = 21.2$  keV) with a 2.950 eV pass energy and at 0.005 eV energy steps. Gold wires were attached to

the samples to prevent charging. To remove contaminants at the surface of SZY and SCYb, Ar<sup>+</sup> sputtering was performed for 5 min prior to the UPS measurement. The voltage was applied from an external power supply to avoid obscuring cutoff energy.

## Results and discussion

### Ionic and protonic transport numbers in SZY and SCYb

The results of the hydrogen- and steam-concentration cells conducted on SZY and SCYb are shown (Figs. 2 and 3, respectively). The experimental results for the EMF of the hydrogen-concentration cells were in good agreement with those calculated using the Nernst equation. This indicates a unique ionic conduction, and the electronic conductivity is negligible in a wet-hydrogen atmosphere. The results of the steam-concentration cell test show that SZY and SCYb have a lower oxide-ion transport number than proton transport number (Table 1). Based on these results, the effect of platinum precipitation on the conductivity of SZY and SCYb was investigated at 800 °C or lower where proton conduction was dominant.

### Phase identification of Pt-SCYb by XRD

The XRD patterns of Pt-SCYb sintered at different temperatures are provided (Fig. 4a, b), and all show a single-phase perovskite-type structure. The lack or presence of the platinum peak at  $2\theta = 39.8^\circ$  (Fig. 4b) indicates that the sintering temperature of 1150 °C causes no precipitation of metallic platinum, and that temperatures of 1200 °C or higher cause the precipitation of metallic platinum particles as a secondary phase. The color of the specimen is consistent with either the absence or presence of the platinum precipitates. When sintered at 1150 °C or lower, the color remained pale yellow which is indicative of the absence of platinum precipitates. Sintering at 1200 °C or higher changes the color to dark brown or black, indicating the presence of platinum precipitates. As described above, platinum must be dissolved into the perovskite phase at the stage of sintering in air to form platinum nanoparticles for conductivity to be measured in different gas atmospheres. Therefore, the following electrical conductivity measurement was carried out using samples sintered at 1150 °C for Pt-SCYb and SCYb. Pt-SZY and SZY were prepared as described previously and sintered at 1350 °C, and the color of Pt-SZY is blue caused by a solid solution platinum as reported as [21], and the color of SZY is white. The relative densities of the specimens were as follows: Pt-SCYb, 70.2%; Pt-SZY, 83.7%; SCYb, 69.7%; and SZY, 59.8%. These comparatively high

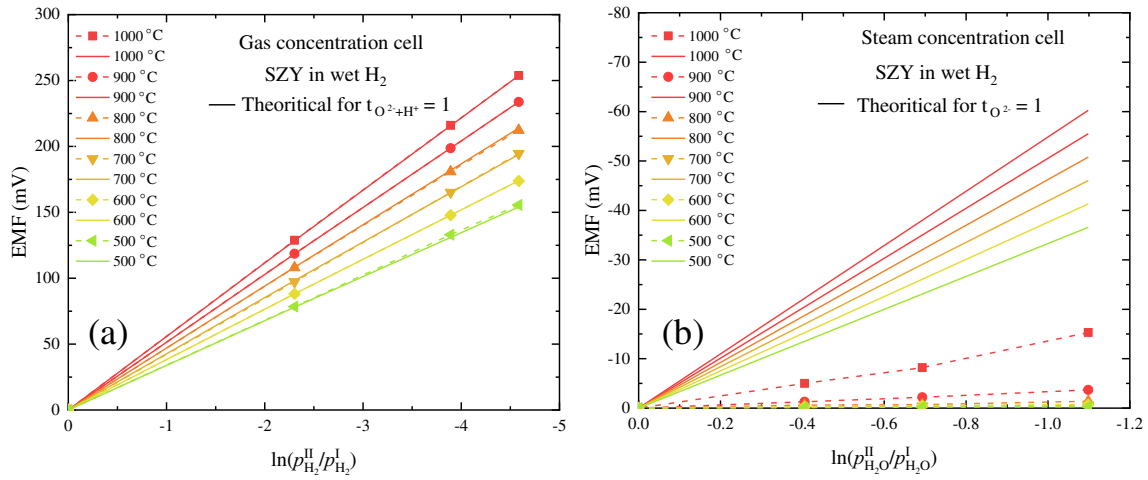


**Fig. 2** Results from **a** the gas concentration cell test and **b** steam concentration cell for SZY. Solid lines represent theoretical values, and the dashed lines represent experimental values

relative densities on platinum-doped samples may be caused by the platinum which might work as a combustion-promoting catalysis. The lattice constants and cell volume of these samples are summarized in Table 2.

### Effect of dissolved/precipitated platinum on the electrical conductivity of SZY and SCYb

Figure 5 compares the electrical conductivity of Pt-SZY and Pt-SCYb with the platinum-free oxides at 800 °C in changing inflow gases ( $p_{\text{H}_2\text{O}} = 1.9$  kPa), together with photos of Pt-SCYb annealed in each atmosphere. The grain boundary blocking is often a problem in such perovskites, especially with the zirconate system; however, the effect is less severe in this measurement temperature (800 °C). The following

equation was used to correct the measured electrical conductivity with the limited relative density to the full-density conductivity:

$$\sigma_{\text{mea}} = 2(0.01d_{\text{rel}} - 0.5) \times \sigma_{\text{ful}} \quad (9)$$

where  $\sigma_{\text{mea}}$ ,  $\sigma_{\text{ful}}$ , and  $d_{\text{rel}}$  are the measured conductivity, full-density conductivity, and relative density, respectively [24].

As shown (Fig. 5a), Pt-SZY and SZY have similar conductivity in wet air and argon atmospheres, but the conductivity of Pt-SZY showed a significant drop when the atmosphere changed from wet argon to wet 1%  $\text{H}_2$ . On the other hand, undoped SZY showed no significant drop in conductivity upon the change between wet argon and 1%  $\text{H}_2$  gases. Consequently, in 1%  $\text{H}_2$ , the conductivity of Pt-SZY was approximately one fifth of that of undoped SZY. In the case of

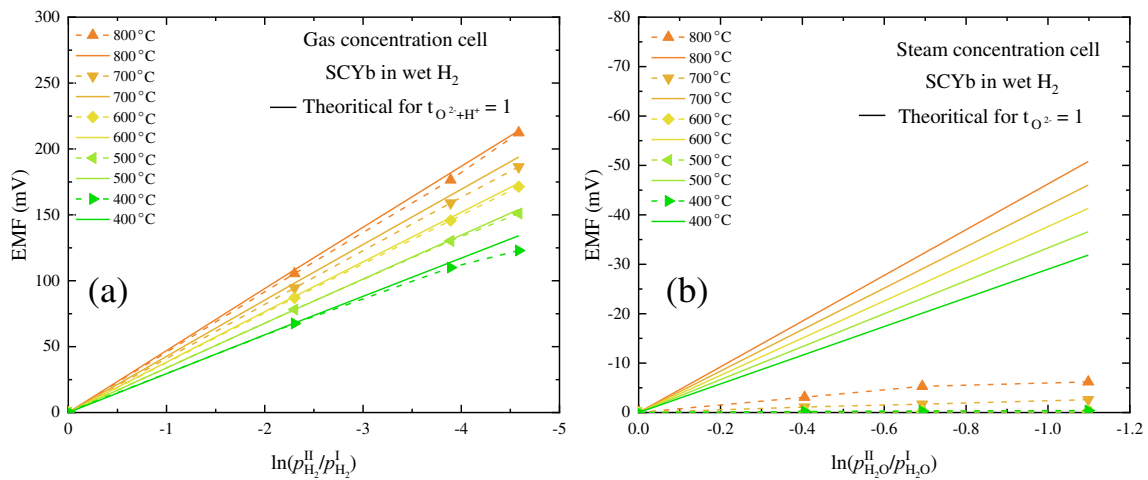


**Fig. 3** Results from **a** the gas concentration cell test and **b** the steam concentration cell for SCYb. Solid lines represent theoretical values, and the dashed lines represent experimental values

**Table 1** Transport number of SZY, SCYb, and Pt-SCYb in wet H<sub>2</sub> atmosphere

Composite relative density	SrZr <sub>0.9</sub> Y <sub>0.1</sub> O <sub>3-δ</sub> 95.1%			SrCe <sub>0.95</sub> Yb <sub>0.05</sub> O <sub>3-δ</sub> 95.0%			0.5vol.%Pt-SrCe <sub>0.95</sub> Yb <sub>0.05</sub> O <sub>3-δ</sub> 96.7%		
	$t_{e^-}$	$t_{H^+}$	$t_{O^{2-}}$	$t_{e^-}$	$t_{H^+}$	$t_{O^{2-}}$	$t_{e^-}$	$t_{H^+}$	$t_{O^{2-}}$
1000 °C	0.00	0.75	0.25	–	–	–	–	–	–
900 °C	0.00	0.93	0.07	–	–	–	–	–	–
800 °C	0.00	0.97	0.03	0.03	0.84	0.13	0.00	0.93	0.07
700 °C	0.01	0.98	0.01	0.04	0.90	0.06	0.00	0.97	0.03
600 °C	0.00	0.98	0.02	0.01	0.98	0.01	0.01*	0.96*	0.03*
500 °C	0.00	0.99	0.01	0.00	1.00	0.00	0.03*	0.94*	0.03*
400 °C	–	–	–	0.00	1.00	0.00	0.00*	0.81*	0.19*

\* Since EMF plots are bending at high H<sub>2</sub> concentration under 600 °C of Pt-SCYb, these  $t_i$  are estimated under 10% H<sub>2</sub>

Pt-SZY, we previously reported that platinum nanoparticles are precipitated out in a wet 1% H<sub>2</sub> atmosphere homogeneously in the bulk, as confirmed by TEM and XAFS measurements, resulting in a color change of the specimen (shown in the inset of Fig. 2 in ref. [21]). We also reported the observed development of a negatively charged space-charge layer in SZY at the interface with metallic platinum through the use of electron holography (Fig. 5 in ref. [21]). We explained that the decrease in conductivity can be attributed to the formation of a negatively charged space-charge layer accompanying the depletion of protons in SZY at the interface with the platinum nanoparticles [20, 21] (illustrated in Fig. 1 (a')).

Change in the conductivity of Pt-SCYb and SCYb in response to the change of the gas atmospheres is shown in Fig. 5b. The conductivity of Pt-SCYb is lower than that of SCYb in wet air and argon. Upon the change of the gas to wet 1% H<sub>2</sub>, both the conductivities of Pt-SCYb and SCYb increase and the extent of the increase is larger in Pt-SCYb. In regard to the increased conductivity of undoped SCYb in wet hydrogen atmosphere, Bonanos and Pollsen explained this phenomenon that exposure to hydrogen results in the reduction of Ce<sup>4+</sup> to Ce<sup>3+</sup>, and the reduced cerium does not lead to the apparent development of n-type conductivity but works as the acceptor to increase the proton concentration [15, 16]. On the other hand, the color of the Pt-SCYb specimen turned to dark brown

upon exposure to 1% H<sub>2</sub>, suggesting the formation of precipitated platinum nanoparticles. The result of TEM observation of the Pt-SCYb after exposure to 1% H<sub>2</sub> (Fig. 6) shows that platinum nanoparticles were precipitate in the bulk similar to Pt-SZY. Therefore, the markedly larger increase of the Pt-SCYb than SCYb upon exposure to wet 1% H<sub>2</sub> is attributed to the effect of precipitation of the platinum nanoparticles. In Fig. 5b, we can see two-stepwise change in conductivity for the change of the gas atmosphere from Ar to 1% H<sub>2</sub> in Pt-SCYb. The relaxation of the conductivity may thus include equilibration of the defects to the change of gas atmospheres and the influence from the precipitation of platinum.

One possible explanation for the increased conductivity in 1% H<sub>2</sub> from that in Ar is that the precipitation of platinum nanoparticles appears to result in a conductivity enhancement, corresponding to the case shown in Fig. 1 (c'). Comparison of the conductivities of Pt-SCYb and SCYb (Fig. 5b), however, leads to a different conclusion. Firstly, the conductivity of the specimen with a solid solution of platinum was approximately one order of magnitude lower under air and argon atmospheres relative to that of undoped SCYb. Secondly, in the wet 1% H<sub>2</sub> atmosphere, the conductivity of Pt-SCYb reached a level similar to that of SCYb. From these, the apparent increase in conductivity upon the gas change from argon to 1% H<sub>2</sub> can be partly explained by the decreased conductivity

**Fig. 4** XRD patterns of Pt-SCYb sintered at different temperatures from 1100 to 1600 °C, **a** in the range of  $2\theta = 10^\circ$  to  $80^\circ$  and **b** magnification at around  $2\theta = 40^\circ$

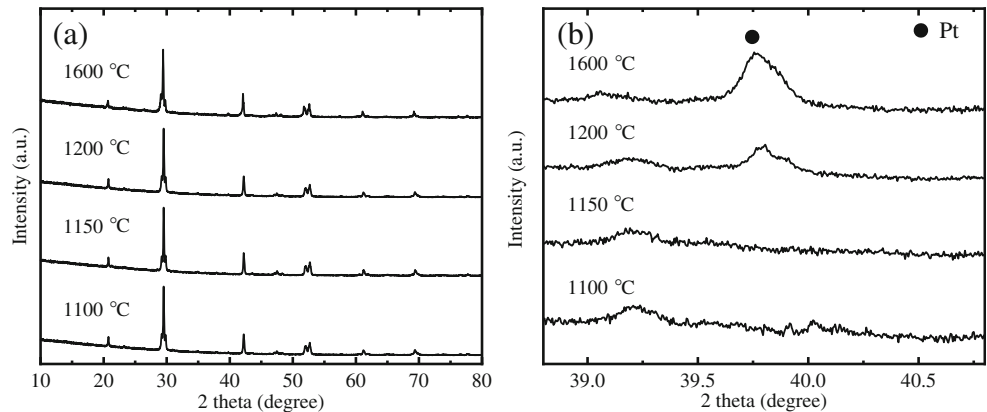


**Table 2** The lattice constants and cell volume

Samples	$a$ (nm)	$b$ (nm)	$c$ (nm)	$V$ (nm <sup>3</sup> )
Pt-SCYb	0.8568	0.5994	0.6125	0.3145
SCYb	0.8579	0.6001	0.6134	0.3158
Pt-SZY	0.5819	0.5800	0.8220	0.2774
SZY	0.5825	0.5808	0.8219	0.2780

of Pt-SCYb in air-argon atmosphere via the dissolution of platinum into SCYb. Recovery of the conductivity to approximately the same level of SCYb can be achieved upon exposure in 1% H<sub>2</sub> atmosphere. The Arrhenius plot of the conductivity of Pt-SCYb and SCYb in wet argon and wet 1% H<sub>2</sub> is shown (Fig. 7). The conductivity was determined by waiting until the value stabilized, and thus, the values are different from those shown in Fig. 5, particularly in the case of the conductivity of SCYb in wet 1% H<sub>2</sub>. The trend explained above is also applicable for the conductivity of Pt-SCYb, which is lower in argon and similar in 1% H<sub>2</sub> to that of SCYb throughout the range of temperatures used in the experiment.

In regard to the effect of platinum dissolution on the conductivity, Shimura et al. reported that the electrical conductivity of BaCe<sub>0.9</sub>Y<sub>0.1</sub>O<sub>3- $\delta$</sub>  perovskite oxide was reduced in an oxidative atmosphere with a dissolved transition metal [25]. We obtained similar results with various perovskites [26]. (This work is under submission, and the selected results are shown in supporting information in Fig. S1). The conductivity is decreased in many cases, while the conductivity is almost unchanging in some cases, by the doping of transition metals, and the degree of conductivity degradation differs by the sort of transition metals and perovskites with no systematic correlation. It is possible to assume that Pt dissolution is working in the same way as thus the transition metal, i.e., the proton conductivity is highly degrading in the case of SCYb and less degrading in the case of SZY.

The increased conductivity of Pt-SCYb upon exposure to 1% H<sub>2</sub> can be explained by generation of electronic charge carriers. However, the temperature dependence of the conductivity of Pt-SCYb in 1% H<sub>2</sub> is similar to that of SCYb (Fig. 7). In addition, as depicted in Fig. 8a, b, the impedance plot of Pt-SCYb and SCYb is similar in both shape and frequency. These suggest that the charge carriers of Pt-SCYb are the same as those in undoped SCYb in 1% H<sub>2</sub>, namely protons with oxide ions as a minor component. To ensure this understanding, we tried to increase the relative density of Pt-SCYb and a change of the preparation condition and increase in the amount of added ammonium nitrate, resulted in the high densification to allow the use for the hydrogen- and steam-concentration cell test. The result is shown (Fig. 9), and the obtained transport numbers are summarized (Table 1). The results indicate that the Pt-SCYb in hydrogen atmosphere, i.e., the platinum nanoparticle-precipitated SCYb, has negligible electronic conductivity and the charge-carrier species are almost the same as those in Pt-undoped SCYb. It is thus conclusive that the increased conductivity of Pt-SCYb is accounted by the proton conduction with minor contribution of oxide ion in the same level as those in the original Pt-undoped SCYb. For Pt-SCYb, the conductivity in the second argon and air atmospheres does not recover to exactly the same value unlike in the case of SCYb. We believe that the precipitation and dissolution of platinum in the Pt-SCYb perovskite structure may have a mechanically or chemically destabilizing effect on the bulk structure.

In the case of Pt-SCYb, the introduction of heterointerfaces with platinum nanoparticles upon exposure to 1% H<sub>2</sub> led to almost no decrease in conductivity relative to that of SCYb. This is a marked difference from the Pt-SZY case in which the protonic conductivity decreased, presumably because of the heterointerfaces with platinum nanoparticles in 1% H<sub>2</sub>. The depletion of protonic charge carriers in Pt-SZY has been assumed to be

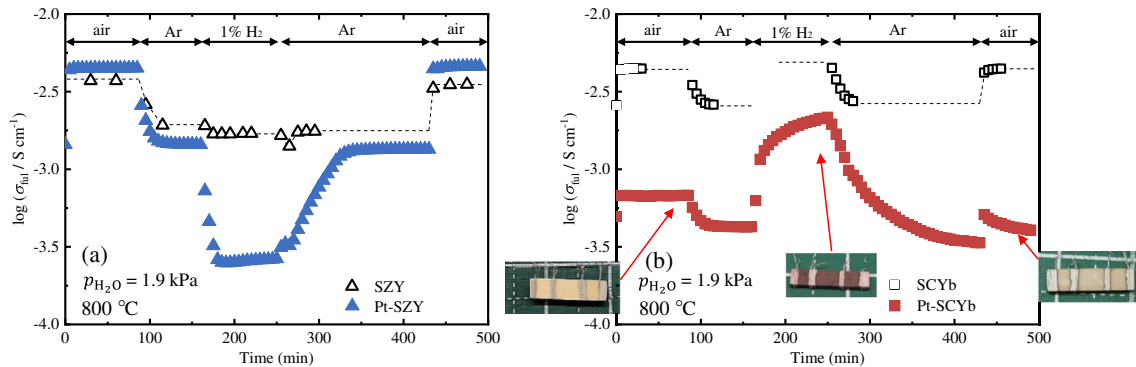
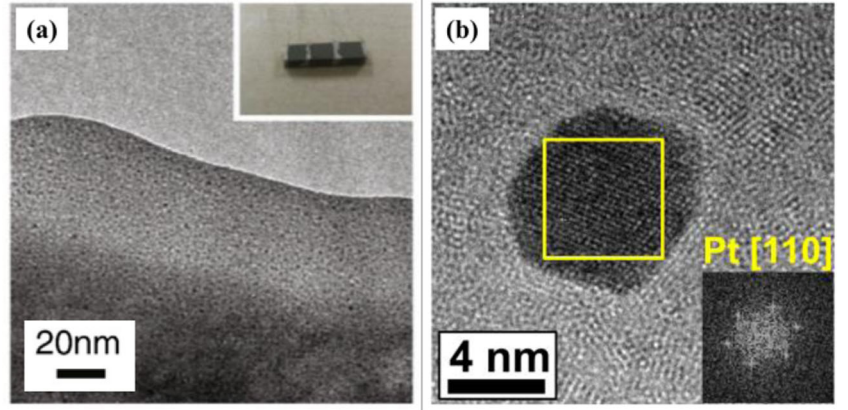


**Fig. 5** Electrical conductivity measurements for **a** Pt-doped/undoped SZY and **b** Pt-doped/un-doped SCYb as a function of time in wet Ar, air, and 1% H<sub>2</sub> gas atmospheres ( $p_{\text{H}_2\text{O}} = 1.9$  kPa). The plotted conductivities were corrected to the full-density conductivity by applying Eq. (9)



**Fig. 6** **a** TEM image of hydrogen-treated Pt-SZY, excerpt from reference [21] following Elsevier's copyright policy. **b** TEM image of hydrogen-treated Pt-SCYb



the cause for the reduced conductivity (Fig. 1 (a')). If this assumption is correct, then there is no effect on SCYb in regard to the proton concentration on the formation of platinum nanoparticles. This result is consistent with the high electrocatalytic activity of platinum electrodes on SCYb in comparison with that on SZY [22]. One possible explanation, based on the band bending model (shown in ref. [20] and in Fig. 1), is that the work functions of SCYb and metallic platinum are very close to each other so that no electron transfer at the Pt/SCYb interface will take place. Thus, the SCYb phase is not electrically charged, resulting in no change in the proton concentration, as seen with the case shown in Fig. 1 (b'). To see if this assumption is true, the work function of SZY and SCYb was measured by UPS reported in the next section.

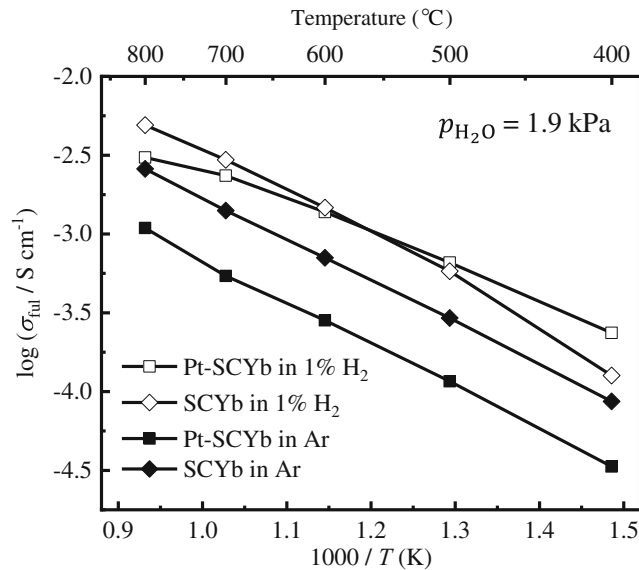


**Fig. 7** Comparison of the conductivities of Pt-SCYb and SCYb in wet Ar and 1% H<sub>2</sub> gas atmospheres ( $p_{\text{H}_2\text{O}} = 1.9$  kPa). The plotted conductivities were corrected to the full-density conductivity by applying Eq. (9)

### Determination of work function by UPS

Figure 10a shows the UPS spectra of SZY with  $-5.0$  eV applied by an external power source. For p-type semiconducting oxides, the work function cannot be estimated directly, and the obtained spectra indicate only the ionization energy of the oxide by the following equation:

$$E_i = h\nu - (E_{\text{cutoff}} - E_{\text{VBM}}) \quad (10)$$

where  $E_i$ ,  $h$ ,  $\nu$ ,  $E_{\text{cutoff}}$ , and  $E_{\text{VBM}}$  are the ionization energy, Planck constant, frequency, cutoff energy, and the top of valence band energy, respectively. The energetic relationship among these parameters is shown (Fig. 11).  $E_{\text{cutoff}}$  and  $E_{\text{VBM}}$  were obtained from the intersection of the extrapolation of the highest-energy edge and lowest edge and the baseline of the UPS spectra. In SZY,  $E_{\text{cutoff, SZY}}$  and  $E_{\text{VBM, SZY}}$  were estimated at 12.68 eV and  $-1.32$  eV, respectively, and so,  $E_{i, \text{SZY}}$  was calculated at 7.2 eV from Eq. (10). The Fermi level of SZY, which is a p-type semiconductor, is located near the acceptor level. When the Fermi level is higher than the top of the valence band by 1.0 V, the work function of SZY can be estimated to be approximately 6.2 eV. How the change in the top of the valence band relative to Fermi level, expressed by  $\Delta E$ , affects the concentration of electronic defects, i.e., electron hole in this case, can be estimated from Eq. (11).

$$p/p_0 = \exp\left(\frac{-\Delta E}{k_B T}\right) \quad (11)$$

where  $p_0$  is the concentration of electron hole and  $p$  is that after the shift of the top of the valence band by  $\Delta E$ .  $k_B$  and  $T$  are Boltzmann constant and absolute temperature. According to the UPS results, the gap of  $E_{\text{VBM, SZY}} - E_{F, \text{SZY}}$  of bulk is  $-1.0$  eV, and  $E_{\text{VBM, SZY}} - E_{F, \text{SZY}}$  of interface is  $-1.6$  eV, and thus,  $\Delta E_{\text{SZY}}$  is 0.6 eV. By applying Eq. (11), the hole concentration differs by three orders of magnitude between the bulk and interface. Proton is in equilibrium electron hole represented by Eq. (5), and thus, its concentration is lowered at the interface with platinum.

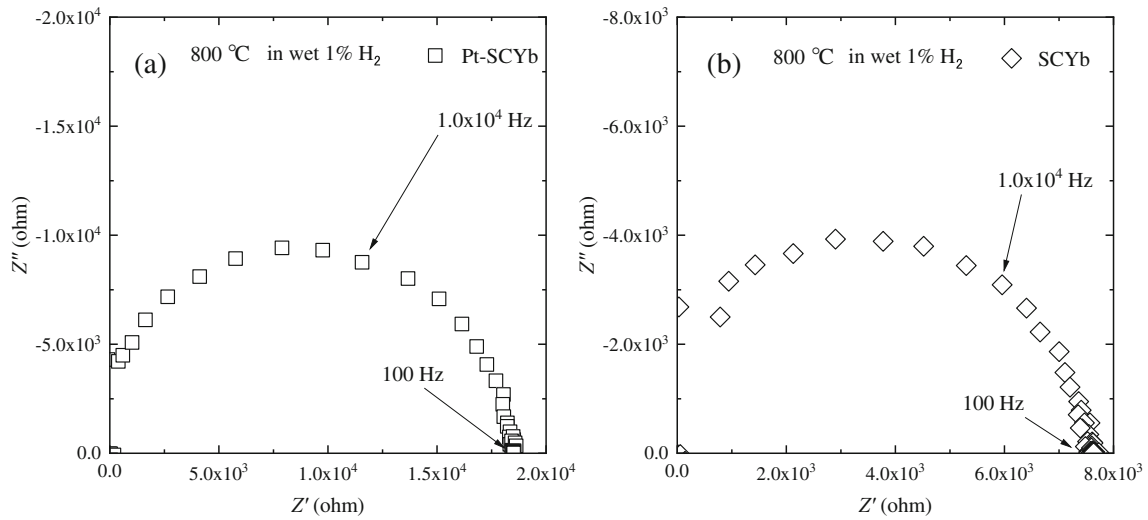


**Fig. 8** Nyquist plots of **a** Pt-SCYb and **b** SCYb in wet 1% H<sub>2</sub> gas atmosphere ( $p_{\text{H}_2\text{O}} = 1.9$  kPa)

Figure 10b shows the UPS spectra of SCYb with  $-5.0$  eV applied by an external power source. In SCYb,  $E_{\text{cutoff, SCYb}}$  and  $E_{\text{VBM, SCYb}}$  were estimated at 12.19 eV and  $-1.51$  eV, respectively, and  $E_{\text{i, SCYb}}$  was calculated at 7.5 eV. Therefore, the work function of SCYb can be estimated to be 6.5 eV. The work function of platinum is 5.6 eV [27] which is smaller than that of SZY and SCYb, and so, both materials should be equally negatively charged at the interface with platinum nanoparticles. We have assumed in the above section that the Fermi levels are similar between SCYb and Pt (Fig. 1 (b')), but this is not the case, and the illustration shown in Fig. 1 (a') is applicable for Pt/SZY and for Pt/SCYb.

Based on these experimental results, another explanation is needed that satisfies the assumption that no depletion of protonic charge carriers occurs under negative charges for the case of SCYb, shown in Fig. 1 (a'). In the case of Pt-SZY, the negative charge is considered to be compensated by reduction of electron hole concentration and according proton

depletion as explained above. One possibility for little depletion of proton in SCYb is that instead of electron hole,  $\text{Ce}^{4+}$  can accept the negative charge (i.e., electron from platinum) to be reduced to  $\text{Ce}^{3+}$ , compensating the development of negatively charged space-charge layer in Pt-SCYb to maintain the proton concentration.  $\text{Ce}^{4+}$  can be reduced more easily than  $\text{Zr}^{4+}$ , and this difference may lead to a change in conductivity. Density functional theory calculations are currently being carried out to examine this hypothesis; the obtained partial DOS of strontium cerate and zirconate is represented as supporting information (Figs. S2 and S3). According to the pre-calculations, both Zr 4d and Ce 4f orbitals form hybrid orbitals with O 2p at both the conduction band and the valence band. One possibility is that  $\text{Ce}^{4+}$  can receive electrons from platinum in order to compensate for the negative charge and prevent a decrease in proton concentration. This speculation is consistent with the explanation made by Bonanos and Pollsen for the increasing conductivity of SCYb by decreasing partial

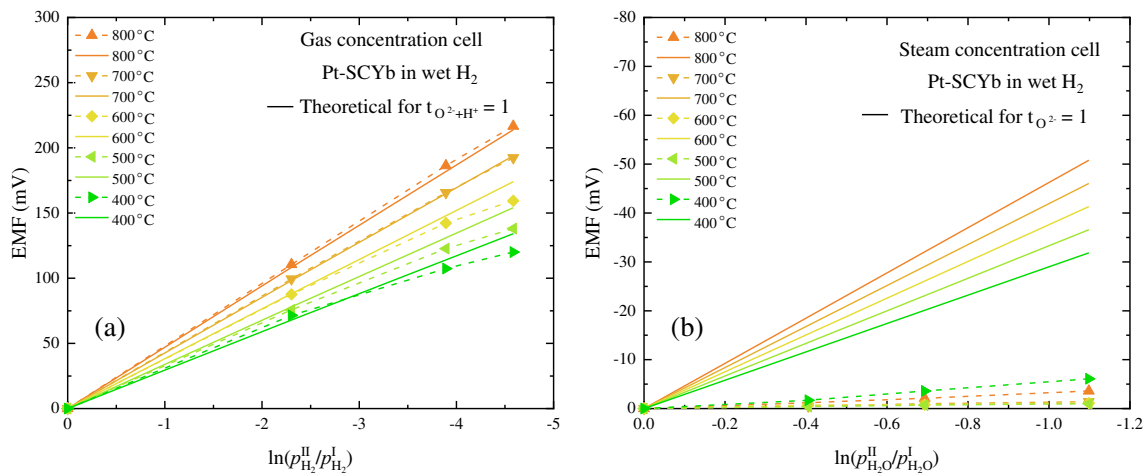
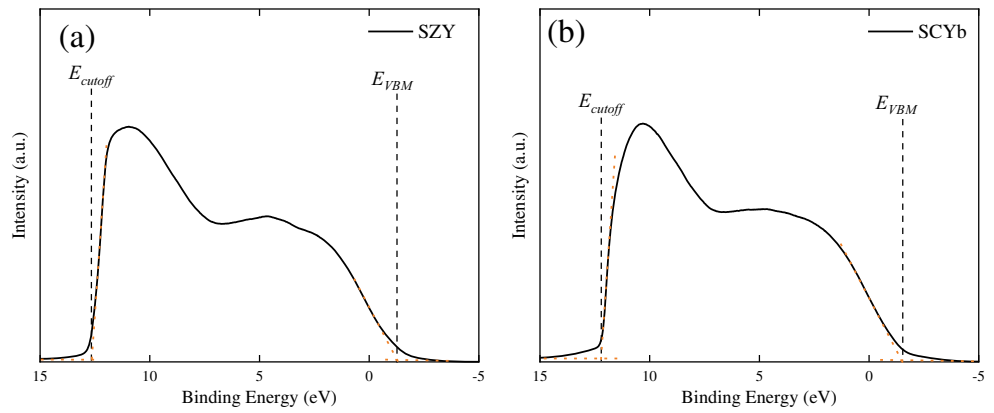


**Fig. 9** **a** The result of gas concentration cell test and **b** steam concentration cell by densified Pt-SCYb. The solid lines represent the theoretical value, and the plots represent experimental values, respectively

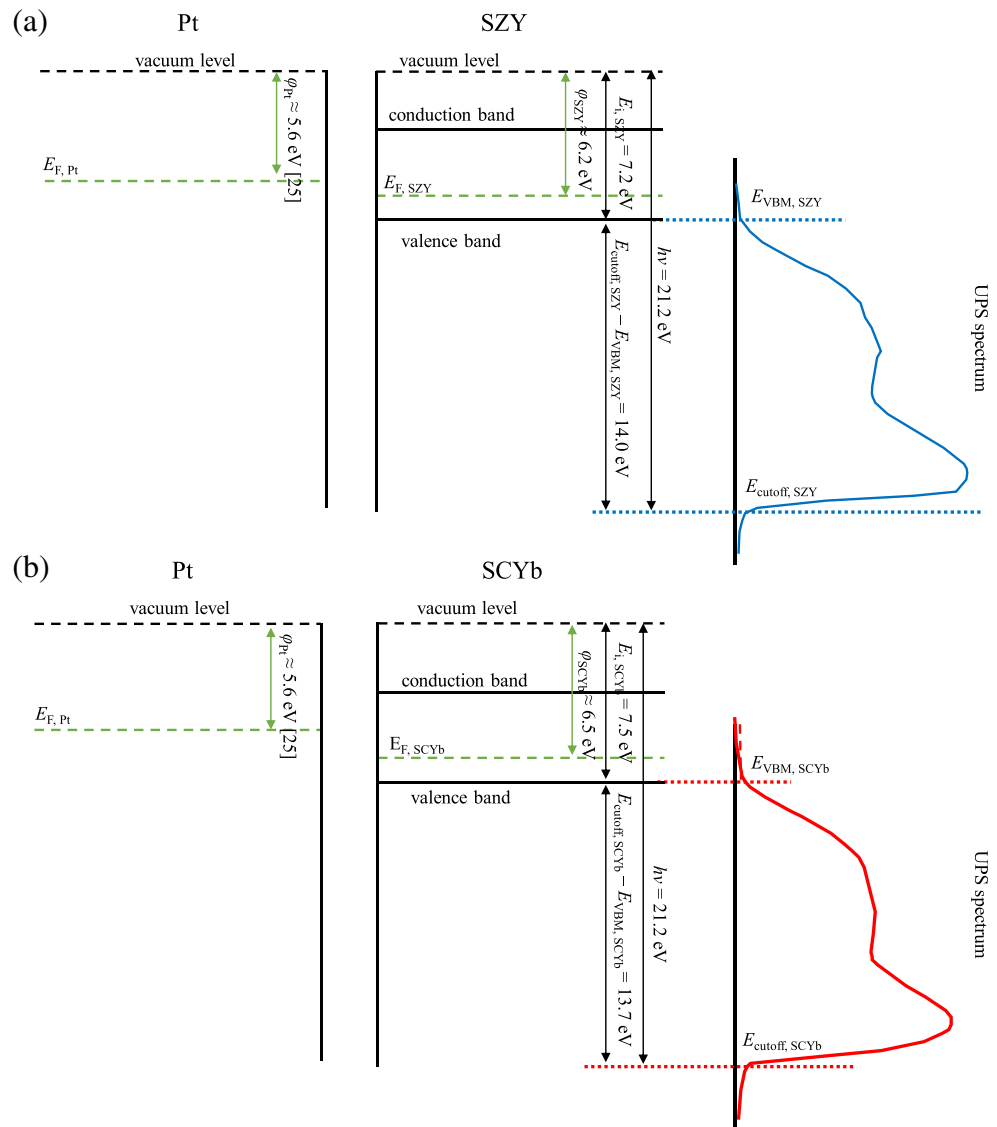
**Fig. 10** UPS spectra of **a** SZY and **b** SCYb with  $-5.0$  eV applied by external power source



pressure of oxygen to be originated by  $\text{Ce}^{3+}$  that works as acceptor to increase the proton concentration [15, 16]. Although more detailed study on this will be necessary, reduction of cerium for the compensation of the negative charge

developed in SCYb at the interface is a possibility to explain the experimentally observed maintenance of proton conductivity in contact with platinum, which is the most significant finding in this report in comparison with Pt-SZY case.

**Fig. 11** Schematic diagram of the electronic band structure for **a** Pt and SZY and **b** Pt and SCYb, with UPS spectra also shown



## Conclusion

The effect of platinum precipitation/dissolution at the heterointerfaces of SCYb and SZY proton-conducting perovskites was investigated. Contrary to the observations for Pt-SZY, Pt-SCYb showed a relative increase in electrical conductivity upon changing the gas atmosphere from wet Ar to 1% H<sub>2</sub>. However, this increase was attributable not to a positive effect of platinum at the interface, but rather to recovery of the conductivity to the original SCYb in a wet hydrogen atmosphere. The UPS results indicate that both SZY and SCYb have a higher work function than platinum, and hence, the oxides should be negatively charged in the vicinity of the platinum/oxide heterointerfaces. This work has demonstrated that the Pt/SZY interface causes decrease in protonic charge carriers, in contrast to the Pt/SCYb interface, which does not affect the proton conductivity. The reason for this marked difference between Pt-SZY and Pt-SCYb is still not clear, and how SCYb can be negatively charged without losing proton conductivity is a question for future study.

**Acknowledgements** This study was supported by World Premium International Research Center Initiative (WPI), MEXT, Japan and the Kyushu University Platform of Inter/Transdisciplinary Energy Research (Q-PIT), JSPS Core-to-Core Program, A. Advanced Research Networks, Partnerships for International Research and Education (PIRE) and A.L. and L.W.M. acknowledge support from the National Science Foundation under grant OISE-1545907. Dr. E. Kaveh of Kyushu University (WPI-I<sup>2</sup>CNER) is acknowledged for the measurement of TEM image of Pt-SCYb.

**Publisher's Note** Springer Nature remains neutral with regard to jurisdictional claims in published maps and institutional affiliations.

## References

1. Iwahara H (1996) Proton conducting ceramics and their applications. *Solid State Ionics* 86–88:9–15
2. Duan C, Tong J, Shang M, Nikodemski S, Sanders M, Ricote S, Almansoori A, OHayre R (2015) Readily processed protonic ceramic fuel cells with high performance at low temperatures. *Science* (80- ) 349(6254):1321–1326
3. Bae K, Jang DY, Choi HJ, Kim D, Hong J, Kim BK, Lee JH, Son JW, Shim JH (2017) Demonstrating the potential of yttrium-doped barium zirconate electrolyte for high-performance fuel cells. *Nat Commun* 8:14553
4. Leonard K, Lee YS, Okuyama Y, Miyazaki K, Matsumoto H (2017) Influence of dopant levels on the hydration properties of SZCY and BZCY proton conducting ceramics for hydrogen production. *Int J Hydrog Energy* 42(7):3926–3937
5. Maier J (2001) Ionic and electronic carriers in solids—physical and chemical views of the equilibrium situation. *Solid State Ionics* 143(1):17–23
6. Kreuer KD (1999) Aspects of the formation and mobility of protonic charge carriers and the stability of perovskite-type oxides. *Solid State Ionics* 125(1–4):285–302
7. Sata N, Eberman K, Eberl K, Maier J (2000) Mesoscopic fast ion conduction in nanometre-scale planar heterostructures. *Nature* 408(6815):946–949
8. Maier J (2003) Defect chemistry and ion transport in nanostructured materials: part II. Aspects of nanoionics. *Solid State Ionics* 157(1–4):327–334
9. Kuwata N, Sata N, Tsurui T, Yugami H (2005) Proton transport and microstructure properties in Superlattice thin films fabricated by pulsed laser deposition. *Jpn J Appl Phys* 44(12):8613–8618
10. Maier J (2005) Nanoionics: ion transport and electrochemical storage in confined systems. *Nat Mater* 4(11):805–815
11. Iwahara H, Yajima T, Hibino T et al (1993) Protonic conduction in calcium, strontium and barium zirconates. *Solid State Ionics* 61(1–3):65–69
12. Uchida H, Maeda N, Iwahara H (1983) Relation between proton and hole conduction in SrCeO<sub>3-x</sub>-based solid electrolytes under water-containing atmospheres. *Solid State Ionics* 11(2):117–124
13. Dahl PI, Haugsrud R, Lein HL, Grande T, Norby T, Einarsrud MA (2007) Synthesis, densification and electrical properties of strontium cerate ceramics. *J Eur Ceram Soc* 27(16):4461–4471
14. Ricote S, Bonanos N, Caboche G (2009) Water vapour solubility and conductivity study of the proton conductor BaCe<sub>(0.9-x)Zr<sub>x</sub>Y<sub>0.1</sub>O<sub>(3-x)</sub></sub>. *Solid State Ionics* 180(14–16):990–997
15. Phillips RJ, Bonanos N, Poulsen FW, Ahlgren EO (1999) Structural and electrical characterisation of SrCe<sub>1-x</sub>Y<sub>x</sub>O<sub>c</sub>. *Solid State Ionics* 125(1–4):389–395
16. Bonanos N, Poulsen FW (1999) Considerations of defect equilibria in high temperature proton-conducting cerates. *J Mater Chem* 9(2):431–434
17. Matsumoto H, Hamajima S, Yajima T, Iwahara H (2001) Electrochemical hydrogen pump using a high-temperature-type proton conductor: improvement of pumping capacity. *Solid State Ionics* 145(1–4):25–29
18. Matsumoto H, Hamajima S, Yajima T, Iwahara H (2001) Electrochemical hydrogen pump using SrCeO<sub>3</sub>-based proton conductor: effect of water vapor at the cathode on the pumping capacity. *J Electrochem Soc* 148(10):D121
19. Sakai T, Matsumoto H, Kudo T, Yamamoto R, Niwa E, Okada S, Hashimoto S, Sasaki K, Ishihara T (2008) High performance of electroless-plated platinum electrode for electrochemical hydrogen pumps using strontium-zirconate-based proton conductors. *Electrochim Acta* 53(28):8172–8177
20. Matsumoto H, Furuya Y, Okada S, Tanji T, Ishihara T (2007) Nanoionics phenomenon in proton-conducting oxide: effect of dispersion of nanosize platinum particles on electrical conduction properties. *Sci Technol Adv Mater* 8(6):531–535
21. Matsumoto H, Tanji T, Amezawa K, Kawada T, Uchimoto Y, Furuya Y, Sakai T, Matsuka M, Ishihara T (2011) Nanoprotonics in perovskite-type oxides: reversible changes in color and ion conductivity due to nanoionics phenomenon in platinum-containing perovskite oxide. *Solid State Ionics* 182(1):13–18
22. Matsumoto H, Shimura T, Iwahara H et al (2006) Hydrogen separation using proton-conducting perovskites. *J Alloys Compd* 408–412:456–462
23. Sutija DP, Norby T, Björnbom P (1995) Transport number determination by the concentration-cell/open-circuit voltage method for oxides with mixed electronic, ionic and protonic conductivity. *Solid State Ionics* 77:167–174
24. Nguyen TL, Dokiya M, Wang S et al (2000) The effect of oxygen vacancy on the oxide ion mobility in LaAlO<sub>3</sub>-based oxides. *Solid State Ionics* 130(3–4):229–241
25. Shimura T, Tanaka H, Matsumoto H, Yogo T (2005) Influence of the transition-metal doping on conductivity of a BaCeO<sub>3</sub>-based protonic conductor. *Solid State Ionics* 176(39–40):2945–2950
26. Lee YS, Leonard K, Okuyama Y, Matsumoto H The effect of transition metal doping on the electrical properties of perovskite type proton conductors: (1) alkaline earth cerates. *Submit to Solid State Ionics*
27. Michaelson HB (1977) The work function of the elements and its periodicity. *J Appl Phys* 48(11):4729–4733